Contract No. DAAG29-76-D-0100
D.O. 0622

LASER PULSE SPECKLE EFFECTS

J.C. Leader

McDonnell Douglas Research Laboratories

St. Louis, Missouri 63166

10 October 1977

Final Report for Period 2 June 1977 - 10 October 1977

Approved for public release; distribution unlimited.

Prepared for:
U.S. Army Missile Research and Development Command
In response to:
U.S. Army Research Office
Battelle Columbus Laboratories

The findings of this report are not to be construed as an official Department of the Army position

MCDONNELL DOUGLAS RESEARCH LABORATORIES

MCDONNELL DOUGLAS CORPORATION

D

UNCLASSIFIED

SECURITY CLASSIFICATION OF THIS PAGE (When Data Entered)

REPORT DOCUMENTATION PAGE

READ INSTRUCTIONS BEFORE COMPLETING FORM

1. REPORT NUMBER	2. GOVT ACCESSION NO. 3. RECIPIENT'S CATALOG NUMBER
4. TITLE (and Subtitle) (6) LASER PULSE SPECKLE EFFECTS.	5. TYPE OF REPORT & PERIOD COVERED (9) Final Report. 2 Jun [redacted]-10 Oct [redacted]77
	6. PERFORMING ORG. REPORT NUMBER MDC Q0634
7. AUTHOR(s) (10) J. C. Leader	8. CONTRACT OR GRANT NUMBER(s) (15) DAAG29-76-D-0100 D.A. 05.22
9. PERFORMING ORGANIZATION NAME AND ADDRESS McDonnell Douglas Research Laboratories McDonnell Douglas Corporation St. Louis, MO 63166	10. PROGRAM ELEMENT, PROJECT, TASK AREA & WORK UNIT NUMBERS
11. CONTROLLING OFFICE NAME AND ADDRESS (11) Battelle Columbus Laboratories 505 King Avenue Columbus, Ohio 43201	12. REPORT DATE 10 Oct [redacted]77 13. NUMBER OF PAGES 43 (12) 44p.
14. MONITORING AGENCY NAME & ADDRESS (if different from Controlling Office)	15. SECURITY CLASS. (of this report) Unclassified
	15a. DECLASSIFICATION/DOWNGRADING SCHEDULE

16. DISTRIBUTION STATEMENT (of this Report)

Approved for public release; distribution unlimited

17. DISTRIBUTION STATEMENT (of the abstract entered in Block 20, if different from Report)

18. SUPPLEMENTARY NOTES

19. KEY WORDS (Continue on reverse side if necessary and identify by block number)

laser	structure-function	target-signature
pulse	range-Doppler	LADAR
speckle	rough-surface	

20. ABSTRACT (Continue on reverse side if necessary and identify by block number)

The fluctuations of a scattered laser pulse resulting from the illumination of uncorrelated, rough-surface areas of a target are examined. Amplitude fluctuations are treated as a random process with stationary increments. LADAR range-Doppler images can be degraded by these fluctuations. Field structure functions are calculated for conical targets and a normalized structure function is found to be temporally invariant. Range and Doppler smearing of LADAR target signatures is facilitated by the use of

DD FORM 1 JAN 73 1473 EDITION OF 1 NOV 65 IS OBSOLETE

UNCLASSIFIED

SECURITY CLASSIFICATION OF THIS PAGE (When Data Entered)

407 080

20. ABSTRACT (Continued)

the local degree of coherence function which is simply related to the normalized structure function for targets having normalized local homogeneity (such as cones).

PREFACE

This report is an account of the work performed by the McDonnell Douglas Research Laboratories on Laser Pulse Speckle Effects for the U.S. Army Missile Research and Development Command (MIRADCOM) under subcontract to the Battelle Columbus Laboratories (Scientific Services Agreement D.O. No. 0522) and authorized by the Army Research Office Contract DAAG29-76-D-0100. The work was performed in the Chemical Physics Laboratory, managed by Dr. C. J. Wolf. The principal investigator was Dr. J. C. Leader; Mr. J. M. Putnam was responsible for the computer programming. The contracting officer's technical representative was Dr. John P. Stettler, Physical Sciences Directorate, MIRADCOM, Huntsville, AL.

This technical report has been reviewed and is approved.

C. J. Wolf by D. P. Ames

C. J. Wolf
Chief Scientist, Chemical Physics
McDonnell Douglas Research Laboratories

D. P. Ames

D. P. Ames
Staff Vice President
McDonnell Douglas Research Laboratories

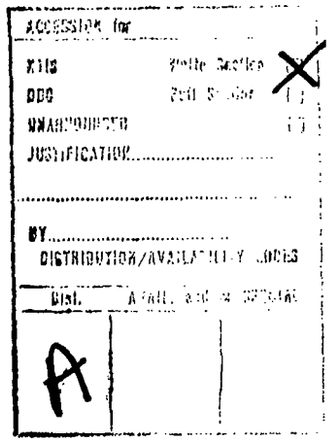

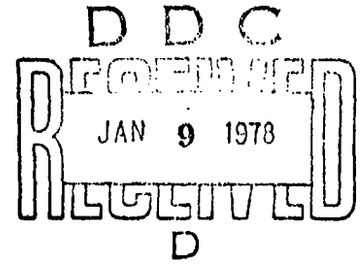

TABLE OF CONTENTS

LIST OF ILLUSTRATIONS

1. OBJECTIVE AND APPROACH

The objective of this study was to investigate the temporal correlations of laser light scattered by a target illuminated with a laser pulse and assess the effects of these correlations on the time/speckle-spectrum signature of the target. Because of the limited duration and level-of-effort provided by the Scientific Services Agreement, the investigative approach focused upon analyzing the phenomena from an overall viewpoint and utilized previous analytical and computational tools maximally. To achieve maximum benefits to MIRADCOM in the allocated time period, emphasis was placed upon (a) a physical understanding of the scattering phenomena, (b) a qualitative assessment of the impact of pulse speckle effects upon pulse-Doppler LADAR systems, and (c) the identification of appropriate analytical methods which can be used for more detailed analyses of the statistics of time/speckle-spectrum target images.

2. SUMMARY OF RESULTS

Significant results of this contract study are summarized below. A more detailed outline of analytical and computed results is provided in Sections 4 and 5.

- Target rotation during a pulse interval degrades the performance of a linear FM chirp LADAR range-Doppler system because many speckle lobes are swept by the receiver.
- Intra-pulse speckle can degrade the performance of coherent pulse-train LADAR range-Doppler systems because time samples of the spectra are smeared in range by speckle fluctuations. A priori knowledge of the target's range and velocity can reduce this degradation via suitable data processing.
- The statistical fluctuations of laser light scattered by a three-dimensional target illuminated with a laser pulse are generally non-stationary. However, the fluctuations can be treated as a random process with stationary increments and described by an appropriately defined structure function. Amplitude statistics are generally zero-mean, circular Gaussian.
- An analytical method for calculating (ensemble-averaged) undistorted range/speckle-spectrum signatures and structure functions of conical targets was developed. Calculational limitations imposed by customary, flat-plate target quantization techniques are obviated by this method.
- The surface roughness of conical targets impacts the LADAR time/speckle-spectrum signature most dramatically for laser-beam incident angles approaching the (cone-axis) normal.
- The scattered-field fluctuations resulting from a laser-pulse illuminated, homogeneous, randomly rough cone have normalized local homogeneity (as defined in this investigation).

3. RECOMMENDATIONS

- Detailed, parametric calculations of speckle distortion effects should be performed to assess the maximum mensurational capability (i.e., ignoring other noise effects) of both chirp and coherent pulse-train time/speckle-spectrum LADAR target imaging systems. Results of these calculations should be compared with analogous experimental data, as available, to guide subsequent analytical and experimental efforts.

- Because the scattered-field structure function is central to calculations of range-smearing effects for coherent pulse-train systems, the structure function for non-conical targets (of interest to BMD and MIRADCOM) should be performed to test the similarity of these structure functions with the functional form (see Section 5) found for conical targets.

4. ANALYSIS

4.1 Pulse Speckle Effects on Time/Speckle-Spectrum Signatures

Basically, two types of range-Doppler imaging systems have been proposed to mensurate targets via their time/speckle-spectrum signature. The linear FM chirp system[1] determines the target range by demodulating the received (scattered) chirp pulse so that range is proportional to the frequency of the demodulated signal. Doppler (speckle spectrum) information is obtained by Fourier transforming numerous pulse amplitudes for each range cell. Receiver bandwidth requirements are generally not stressed by this technique. The coherent pulse-train technique relies upon the limited time duration of the pulses comprising the pulse-train to range-resolve the target while the spectrum of fluctuations is sampled by the pulses so that the pulse-train duration determines the spectrum resolution. The receiving system bandwidth is generally determined by the inverse pulse-width for the coherent pulse-train system. The large bandwidths resulting from detailed range resolution requirements stress the current optical receiver technology.

Random, radiation field-fluctuations (producing the irradiance fluctuations commonly known as speckle) result from basically two types of laser scattering phenomena: (1) rough-surface laser scattering reduces the spatial coherence of the laser light such that the scattered field is only partially correlated at different scattering angles,[2] and (2) the illumination of different rough-surface areas decorrelates the scattered field because the rough-surface areas are only partially correlated. Similar coherence losses result from random volume-scattering processes.[3] The coherence losses resulting from scattering angle differences and different illuminated-areas impact, respectively, the linear FM chirp and coherent pulse-train imaging systems.

Because the pulse width of the linear FM chirp range-Doppler imaging system is generally much longer than any target dimension of interest (L/c, where L is the target length and c is the velocity of light), coherence losses resulting from different illuminated areas do not significantly influence this system. However, target rotation during the time the pulse illuminates the target can produce a temporal amplitude fluctuation of the scattered pulse resulting from the changing scattering coordinates of the receiver. The number of spatially de-correlated (i.e., speckle) cells seen by

the receiver during the pulse interval (T_p) is given approximately by

$$N_s = 2\Omega T_p L/\lambda \quad , \tag{1}$$

where Ω is the target rotation rate and λ is the laser wavelength. The frequency uncertainty resulting from these fluctuations is[4]

$$\Delta\nu = 2L\Omega/\lambda \quad . \tag{2}$$

This frequency uncertainty can be comparable with the frequency range determining the length of the target, and thus the range-Doppler image of the target is degraded.

Because the pulse-width of the coherent pulse-train, range-Doppler imaging system is much less than the range dimension of the target (to range resolve it), the number of speckle cells, N_s, subtended during a pulse interval is fractional for most rotation rates of interest at optical wavelengths. Thus, coherence losses resulting from scattering angle changes, during a pulse interval, are negligible. However, because the pulse interval is less than the target dimension, independent rough-surface areas are illuminated as the pulse traverses the target, and the resulting scattered field fluctuations can alter the expected range-Doppler image. Because MIRADCOM is primarily interested in the coherent, pulse-train, range-Doppler imaging system, the remainder of this report is devoted to analysis of the temporal-field fluctuation resulting from the laser illumination of uncorrelated surface areas and their impact upon the time/speckle-spectrum signature.

For simplicity the square-wave pulse train illustrated in Figure 1 is considered, and the classic BMD conical target (also illustrated) is treated. Denoting the incident electric field by $\vec{E}_o(t)$ and the field scattered by the target to point P (at a range, R, from the target) with polarization component j by $E_{sj}(t)$, the average scattered-field intensity is (by definition)

$$\left\langle E_{sj}(t) E^*_{sj}(t) \right\rangle = \frac{|\vec{E}_o(t-R/c)|^2}{4\pi R^2} \, \sigma(t-R/c), \tag{3}$$

where $\sigma(t)$ is the cross section of the target that is illuminated by the pulse at time, t. Speckle effects resulting from uncorrelated, illuminated target areas cause the actual intensity to fluctuate about the mean value predicted by Equation (3). Thus, for a given pulse comprising the pulse train, the magnitude of the actual scattered field could fluctuate in a manner similar to the fluctuations shown in Figure 2. Because the variance of the field fluctuations is dependent upon time, the statistics of the field fluctuations are clearly non-stationary.[5] Arguments similar to those presented in Reference 4 indicate that the field becomes decorrelated in a time interval on the order of a pulse width, T_p.

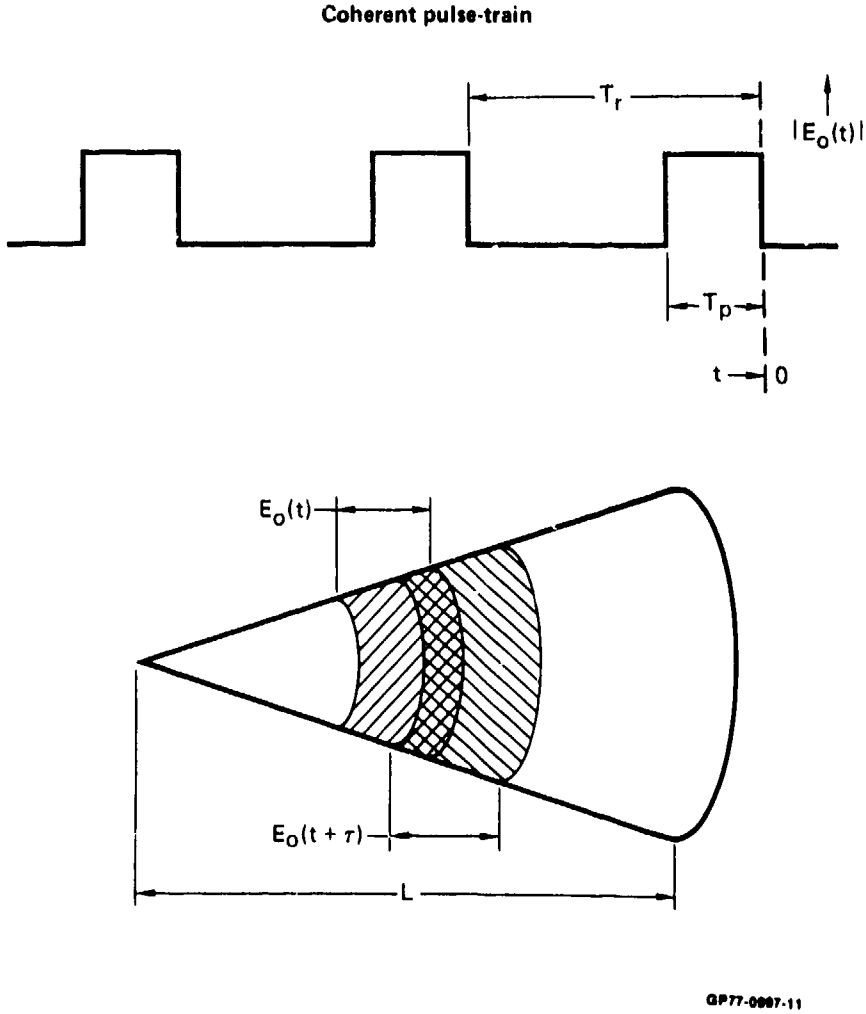

Figure 1 Pulse-train parameters

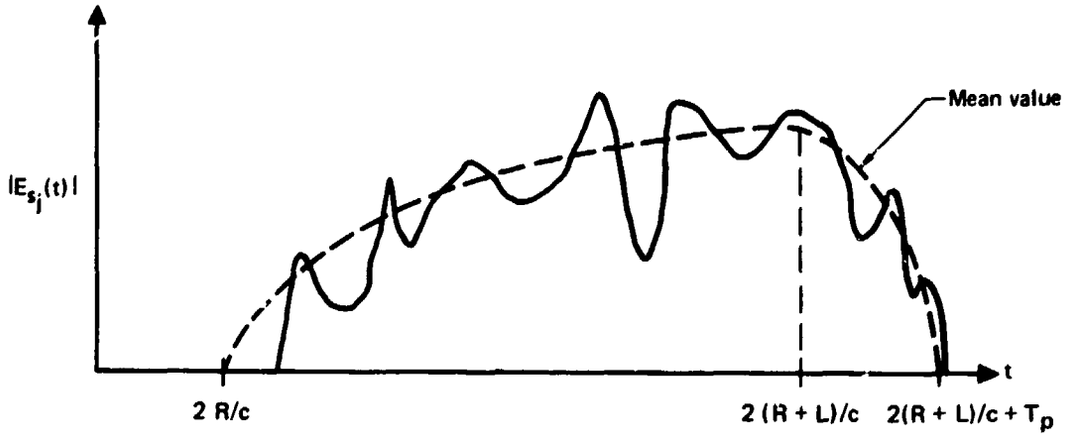

Figure 2 Scattered pulse fluctuations GP77-0007-14

If the scattered field is coherently detected, the intermediate frequency (IF) photocurrent output, x(t), is proportional to the scattered field (neglecting finite aperture effects, shot-noise, and finite bandwidth filtering effects). Thus, assuming that the range rate of the target is zero, the ideal (i.e., uncorrupted by noise and filtering effects) photocurrent signal varies temporally in a manner similar to that shown in Figure 3. The speckle spectrum[6] within a range interval corresponding to a pulse-width (T_p) is obtained by squaring the Fourier transform of some measure of the field (photocurrent) fluctuations resulting from scattering within that range interval. A reasonable measure of the field is provided by the integrated photocurrent output within a pulse interval, i.e.,

$$X(t_n, \Delta R) = \int_{t = 2(R + \Delta R)/c + (n - 1)T_r}^{t = 2(R + \Delta R)/c + (n - 1)T_r + T_p} dt\, x(t) \quad . \qquad (4)$$

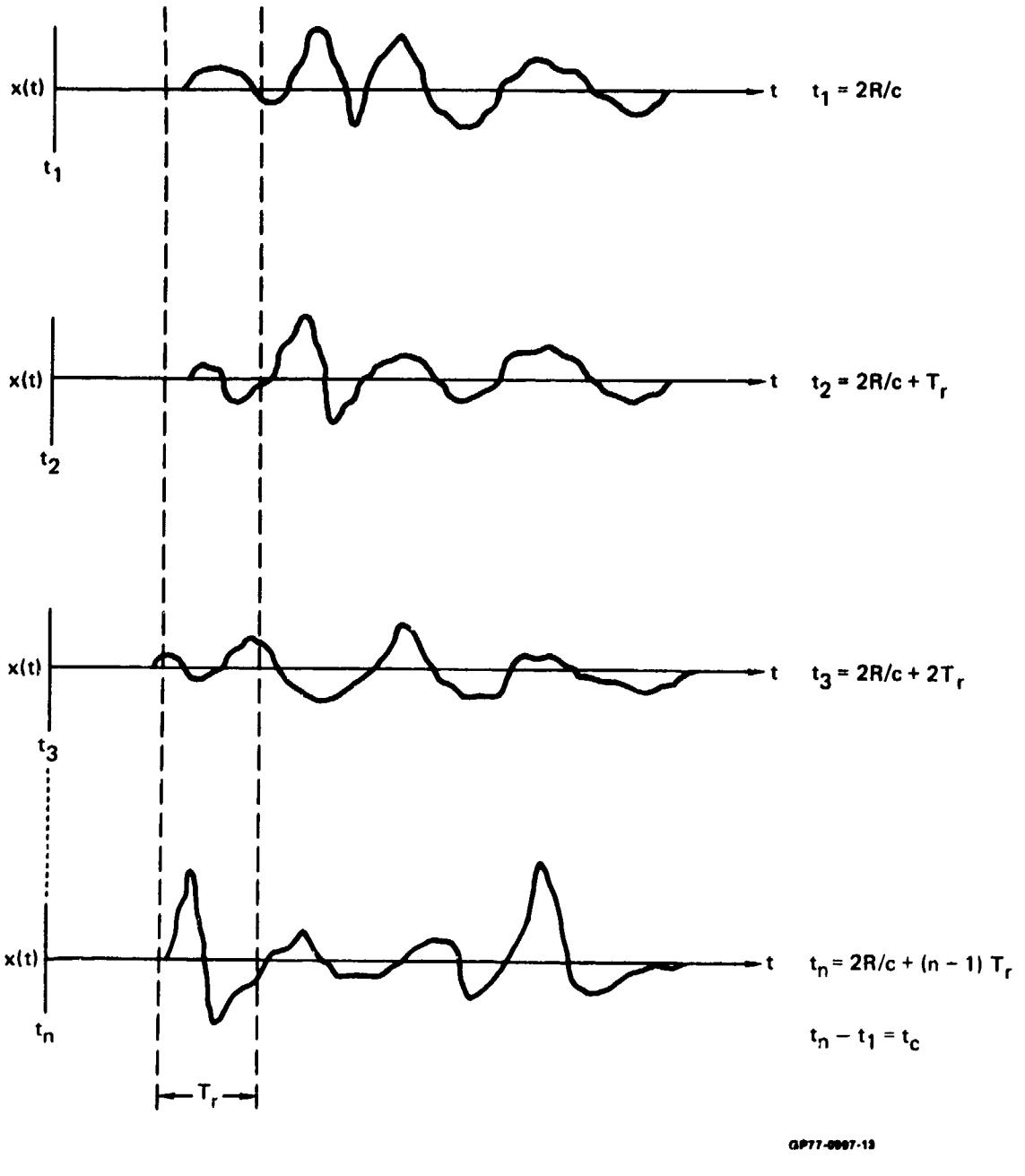

Figure 3 Scattered pulse-train fluctuations

The sampled (discrete) Fourier transform of the field fluctuations is then

$$\tilde{X}_{T_c}(\omega, \Delta R) = \sum_{n=1}^{N} X(t_n, \Delta R) e^{-i\omega t_n} \tag{5}$$

for the N pulses comprising the pulse-train and the square-law spectrum (proportional to the target's cross-range, differential cross section) is

$$S(\omega, \Delta R) = \frac{1}{T_c} \left| \tilde{X}_{T_c}(\omega, \Delta R) \right|^2, \tag{6}$$

where T_c is the coherence time (i.e., duration of the pulse-train). If the nearest part of the target is initially at a range R (at the beginning of the pulse-train) and has a relative velocity,

$$\dot{R} = \frac{dR}{dt} , \tag{7}$$

the appropriate measure of the field fluctuations resulting from the range increment at a range ΔR along the target [corresponding to the static measure provided by Equation (4)] is

$$X(t_n, r) = \int_{t = 2(R + \Delta R)/c + (n - 1)T_r(1 + \dot{R}/c)}^{t = 2(R + \Delta R)/c + (n - 1)T_r(1 + \dot{R}/c) + T_p} dt x(t) . \tag{8}$$

The correction to the integration interval $[(n - 1)T_r\dot{R}/c]$ shown in Equation (8) is negligible for most relative velocities and coherent integration times $[T_c = (n - 1)T_r]$ of interest because of the small value of the ratio $\dot{R}/c$. However, the cumulative effect of this time (range) interval correction $(T_i\dot{R}/c)$ over the incoherent integration time (T_i), required to reduce the variance of the deduced speckle (Doppler) spectrum, is significant because $T_i >> T_c$.

An examination of the systems consequences of intra-pulse speckle does not fall within the purview of this investigation. However, because the time/speckle-spectrum signature consequences of intra-pulse speckle are system dependent, it is worthwhile to itemize a few examples of the types of effects that can be expected.

(1) If the receiving system is designed to time (range) the target by sensing some measure of the arrival time of each pulse (e.g., leading edge, trailing edge, mean, etc.), inaccuracies in the arrival time on the order of a pulse width will result from speckle fluctuations. Thus, a random mixture of adjacent range increment measures of the photocurrent $[X(t_n, \Delta R + R_n)$ where R_n is a random variable with a variance on the order of $cT_p]$ are Fourier transformed to obtain the cross-range spectrum, $S(\omega, \Delta R)$. The resultant time/speckle-spectrum signature is consequently degraded.

(2) If the receiving system establishes fixed range-interval increments to sample field fluctuations [in the manner suggested by Equation (4)], admixtures of adjacent range intervals [as suggested in (1)] in the discrete Fourier transform of Equation (5) can result from receiving system jitter.

(3) If the target's relative velocity is unknown (or improperly estimated) and fixed range increments are used [as suggested in (2)], the incoherent integration process will include square-law spectrum samples from adjacent range intervals. Although the sample spectra are quickly decorrelated in range, the resultant averaged spectrum has a degraded range and frequency resolution.

The examples cited above illustrate the manner in which intra-pulse speckle can influence time/speckle-spectrum signatures. The precise manner in which speckle affects the signature derived from a particular range-Doppler imaging system is obviously dependent upon the details of the system implementation. To analyze speckle effects on any system, however, it is necessary to specify the statistics of the speckle fluctuations. The statistics of intra-pulse speckle are explored below.

4.2 Pulse Speckle Statistics

The probability distribution function (PDF) describing speckle fluctuations can be quite generally described by the Hoyt distribution.[7] However,

because the coherent contribution to the scattered field results from approximately equidistant scattering centers to achieve a coherent superposition (i.e., glint returns), the number of target glints is usually small and spatially limited. Therefore, the ensemble average PDF of the field amplitude for the majority of the time domain of the scattered pulse must have non-circular Gaussian statistics.[8] In fact, because the scattered signal results from rough-surface scattering at various ranges considerably in excess of a laser wavelength, the PDF for each polarization component reduces to circular Gaussian statistics.

Because the statistics of the scattered pulse amplitude are circular Gaussian (i.e., the real and imaginary parts have equal variances), it is sufficient to describe the correlation function of the field to completely specify the statistical description of field fluctuations.[9] However, as noted earlier, the temporal field amplitude fluctuations are statistically non-stationary. Therefore, the correlation function is an inappropriate statistical descriptor of the field amplitude fluctuations. However, because (a) the scattered field amplitude increment, $\left\langle E_{sj}(t) - E_{sj}(t') \right\rangle$ is time independent $\left[\left\langle E_{sj}(t) \right\rangle = \left\langle E_{sj}(t') \right\rangle = 0 \right]$ and (b) a suitably defined structure function (shown below) depends only on the time differences $t - \tau/2$ and $t + \tau/2$, the field fluctuations can be treated as a random process with stationary increments.[10] The appropriate structure function for studying fluctuations of any combination of polarization components of the scattered field is

$$
\begin{aligned}
{}^{j}D_{e}{}^{k}(t,\tau) &\equiv \left\langle [E_{sj}(t + \tau/2) - E_{sj}(t - \tau/2)][E_{sk}(t + \tau/2) - E_{sk}(t - \tau/2)]^{*} \right\rangle \\
&\equiv \left\langle E_{sj}(t + \tau/2)E^{*}_{sk}(t + \tau/2) \right\rangle + \left\langle E_{sj}(t - \tau/2)E^{*}_{sk}(t - \tau/2) \right\rangle \\
&\quad - \left\langle E_{sj}(t + \tau/2)E^{*}_{sk}(t - \tau/2 \right\rangle - \left\langle E_{sj}(t - \tau/2)E^{*}_{sk}(t + \tau/2) \right\rangle .
\end{aligned}
\tag{9}
$$

The structure function defined by Equation (9) characterizes the intensity of fluctuations having a period $\leq \tau$. The structure function can also be expressed in terms of the power spectrum of field fluctuations, ${}^{j}W_{e}{}^{k}(\omega)$, as[11]

$$ {}^{j}D_{e}{}^{k}(t_1 - t_2) = 2\int_{-\infty}^{\infty} [1 - \cos\,\omega(t_2 - t_1)]\,{}^{j}W_{e}{}^{k}(\omega)\,d\omega. \tag{10} $$

Thus, if the power spectrum of field fluctuations is characterized by a $\mathrm{sinc}^2(\omega)$ function, i.e.,

$$ {}^{j}W_{e}{}^{k}(\omega) = \left[\frac{\sin\,(\omega T)}{\omega T}\right]^2, \tag{11} $$

the structure function is given by

$$ {}^{j}D_{e}{}^{k}(\tau) = \begin{cases} \pi/2\ \tau/2T & \tau \leq 2T \\ \pi/2 & \tau > 2T \end{cases} . \tag{12} $$

Because the scattered field consists largely of the incoherent component (by the above arguments), correlations at different time increments result from overlapping illumination areas on the target (see Figure 1). Therefore, the Equation (9) definition reduces to

$$ \begin{aligned} {}^{j}D_{e}{}^{k}(t,\tau) = &\left\langle E_{sj}(t + \tau/2)E^{*}_{sk}(t + \tau/2)\right\rangle + \left\langle E_{sj}(t - \tau/2)E^{*}_{sk}(t - \tau/2)\right\rangle \\ &- 2\left\langle E_{sj}(t + \tau/2)E^{*}_{sk}(t - \tau/2)\right\rangle. \end{aligned} \tag{13} $$

Since the scattered field intensities comprising the right-hand side of Equation (13) are proportional to an appropriate range-resolved target cross section [see Equation (3)], the structure function defined by Equation (13) is clearly a function of time, t. The scattered field is therefore a non-homogeneous random process with stationary increments. However, if an appropriately normalized structure is defined, viz.,

$$ {}^{j}\mathcal{D}_{e}^{k}(t,\tau) \equiv {}^{j}D_{e}{}^{k}(t,\tau)/2\left\langle E_{sj}(t)E^{*}_{sk}(t)\right\rangle \tag{14} $$

and if the normalized structure function is largely time independent within the scattered pulse duration, i.e.,

$$ {}^{j}\mathcal{D}_e^k(t,\tau) \approx {}^{j}\mathcal{D}_e^k(\tau) \text{ for } 2R/c - T_p/2 < t < 2(R+L)/c + T_p/2 \quad , \tag{15} $$

the utility of the structure function analysis for describing pulse amplitude fluctuations is considerably enhanced. Field fluctuations having structure functions that satisfy the Equation (15) relation are defined in this investigation as having normalized local homogeneity in analogy with the standard definition of locally homogeneous random processes. The increased utility of the analysis results from the observation that for most targets of interest,

$$ \left\langle E_{sj}(t)E_{sk}^*(t)\right\rangle \approx \frac{1}{2}\left[\left\langle E_{sj}(t+\tau/2)E_{sk}^*(t+\tau/2)\right\rangle + \left\langle E_{sj}(t-\tau/2)E_{sk}^*(t-\tau/2)\right\rangle\right] \tag{16} $$

$$ \text{for } \tau < \tau_s $$

by the mean value theorem, providing the cross section is sufficiently smoothly varying and τ_s is not too large. Thus, within the range of validity of the Equation (16) approximation, a function analogous to the degree of coherence can be defined, i.e.,

$$ \gamma_{jk}^o(t,\tau) = \frac{\left\langle E_{sj}(t+\tau/2)E_{sk}^*(t-\tau/2)\right\rangle}{\left\langle E_{sj}(t)E_{sk}^*(t)\right\rangle} \tag{17} $$

and expressed in terms of the normalized structure function, i.e.,

$$ \gamma_{jk}^o(t,\tau) \approx 1 - {}^{j}\mathcal{D}_e^k(t,\tau) \qquad \text{for } \tau < \tau_s. \tag{18} $$

The function defined by Equation (17) describes the local correlations of the scattered field and has the normalized properties

$$ 0 \le \gamma_{jk}^o(t,\tau) \le 1 \qquad \gamma_{jk}^o(t,0) \equiv 1 \tag{19} $$

akin to the conventional degree of coherence. Therefore, this function will be called the local degree of coherence. Clearly, if the scattered field has normalized local homogeneity [Equation (15) is valid], the local degree of coherence is temporally invariant, i.e.,

$$\gamma_{jk}^{o}(t,\tau) \overset{\sim}{\sim} \gamma_{jk}^{o}(\tau) \text{ for } 2R/c - T_p/2 < t < 2(R + L)/c + T_p/2. \tag{20}$$

This important property permits the calculation of the deleterious intra-pulse speckle effects (discussed in Section 4.1) from a knowledge of the uncorrupted time/speckle-spectrum signature and the normalized structure function. The remainder of this section examines means for calculating the structure function, normalized structure function, and (as an interesting byproduct) the various resolved signatures of a conical target having various surface-roughness properties. Section 5 provides calculations that demonstrate that conical targets indeed have normalized local homogeneity.

4.3 Conical Target Signature and Structure Function Calculations

If a plane-wave laser pulse-train illuminates a conical target, the intersection of the planar wave-front with the cone describes a conic section (i.e., truncated ellipse or hyperbola). The time/speckle-spectrum signature is proportional to the differential laser radar cross section[6] arising from cross-range elements within the time period of the pulse. The differential cross section of the cross-hatched scattering area illustrated in Figure 4 is proportional to the time/speckle-spectrum signature of the conical target for a time delay 2t and speckle spectrum at x having a differential spectral width dx, for a plane wave incident at the polar angle θ (in the y-z plane). Normalized spectral units of x and $d\sigma/dx$ are used in this investigation as in Reference 12 so that knowledge of the cone radius, spin rate, range, incident angle, wavelength, and laser power permits the calculation of the absolute frequency spectrum in units of power and frequency. The projection of the plane-wave conic intersection onto the base of the cone also describes a conic section. The base plane (i.e., x-y) coordinates of the time and spectrum intersections can be solved using the equation of the plane

$$z = \tan \theta \; y + \ell, \tag{21}$$

where ℓ = z-axis intersection of t, and the cone

$$z = -\alpha \sqrt{x^2 + y^2} + h, \tag{22}$$

where $\alpha = h/R_t$.

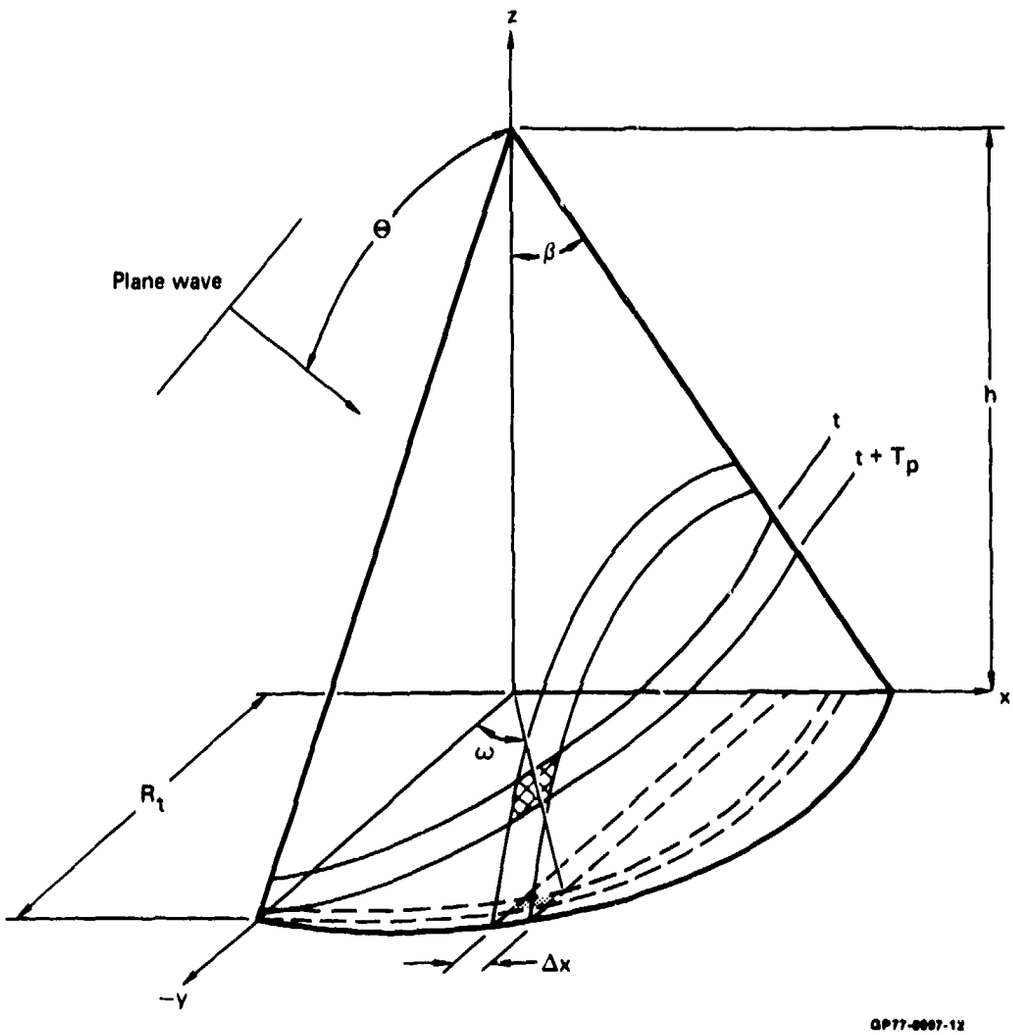

Figure 4 Cone scattering geometry

The intersection of the cone and plane is found from equating Equations (21) and (22), i.e.,

$$y_n = \frac{-\tan\theta(\gamma - \alpha) \pm \sqrt{\alpha^2(\gamma - \alpha)^2 + \alpha^2 x_n^2 \tan^2\theta - \alpha^4 x_n^2}}{(\tan^2\theta - \alpha^2)} , \qquad (23)$$

where $\gamma = \ell/R_t$ and $x_n = x/R_t$, $y_n = y/Rt$ are normalized units having maximum magnitude of unity. The requirement that the intersection lies on the finite cone rather than the infinite cone is mathematically stated

$$x_n^2 + y_n^2 \leq 1. \qquad (24)$$

The differential area, A_I, of the spectrum-pulse width intersection can be found from the relation

$$A_I \cong A_B \csc\beta, \qquad (25)$$

where β is the cone half-angle and A_B is the base projected area. The base projected area can be solved analytically from the expression

$$A_B = \int\sqrt{ax^2 + c}\, dx = \frac{x}{2}\sqrt{ax^2 + c} + \frac{c}{2\sqrt{a}}\log\left(x\sqrt{a} + \sqrt{ax^2 + c}\right) \text{ for } a > 0$$
$$= \frac{x}{2}\sqrt{ax^2 + c} + \frac{c}{2\sqrt{-a}}\sin^{-1}\left(x\sqrt{\frac{-a}{c}}\right) \text{ for } a < 0 , \qquad (26)$$

where a and c are determined from the major and minor axes of the elipse or hyperbola projected upon the base. The differential cross section of the pulse-spectrum intersection is then

$$\frac{d\sigma(t,x,T_p)\big|_{proj}}{dx_p} \cong \frac{\Delta\sigma(t,x,T_p)\big|_{proj}}{\Delta x_p}$$
$$\cong \frac{\csc\beta}{\Delta x} A_B(t,x,T_p)\sigma^o(\omega), \qquad (27)$$

where $\sigma^o(\bar{\omega})$ is the laser cross-section per unit-area of the differential element at the azimuthal angle $\bar{\omega}$. The average azimuthal angle, $\bar{\omega}$, can be found from the relation

$$\bar{\omega}(x) = \frac{1}{2}[\omega(x,t) + \omega(x,t + T_p)], \tag{28}$$

where

$$\omega(x,t) = \tan^{-1}[x_n/y_n(x_n,t)]. \tag{29}$$

The laser cross-section per unit-area, σ^o, can be calculated from the computer code ROSSCO,[13] using the relations in Reference 12 relating the local cone incident and polarization angles to the cone laser incident angle and polarization angles via the azimuthal angle. Cone shadowing effects are accounted for via the caveats

$$\frac{d\sigma(t,x,T_p)|_{proj}}{dx_p} \equiv 0 \tag{30}$$

if

$$\omega(x,t) > \omega_\ell \text{ and } \omega(x,t + T_p) > \omega_\ell \tag{31}$$

and

$$\frac{d\sigma(t,x,T_p|_{proj}}{dx_p} = \frac{\text{csec } \beta}{\Delta x} A_B(t,x,T_p)\sigma^o(\bar{\omega})\, F(\bar{\omega}), \tag{32}$$

if

$$\omega(x,t) < \omega_\ell$$

and (33)

$$\omega(x,t + T_p) > \omega_\ell,$$

where

$$F(\bar{\omega}) = |\omega_{\ell} - \omega(x,t)| \Big/ |\omega(x,t) - \omega(x,t + T_p)|, \tag{34}$$

and ω_{ℓ} is the shadowing azimuthal angle defined in Reference 12.

Equations (23) - (34) and the requisite Equations of Reference 12 when computer implemented with suitable logic required to handle special integration cases arising near the edge of the cone, permit accurate calculations of the ideal time/speckle-spectrum signature for arbitrary scattering geometries, pulse widths and cone roughness conditions. Significantly, this analytical method of calculating signatures does not require subdividing the target into approximate flat-plate areas. Therefore, small pulse-width signatures (required for subsequent structure-function calculations) are facilitated, computer storage requirements are minimal, and the required calculations are extremely rapid. The time (range) resolved cross section is given by

$$\sigma(t,T_p)\big|_{proj} = \int_0^1 dx \frac{d\sigma(t,x,T_p)\big|_{proj}}{dx_p}. \tag{35}$$

Therefore the structure function for the cone is given by

$$\begin{aligned} {}^{j}D_e^{k}(t,\tau) = K[&\sigma(t + \tau/2,T_p;j,k) + \sigma(t - \tau/2,T_p;j,k) \\ &- 2\sigma(t,T_p - \tau;j,k)], \end{aligned} \tag{36}$$

where

$$K = \frac{|\bar{E}_o(t,T_p)|^2}{4\pi R^2}$$

and the normalized structure function is

$$
{}^{j}\mathcal{A}_{e}^{k}(t,\tau) = [\sigma(t + \tau/2, T_p; j,k) + \sigma(t - \tau/2, T_p; j,k) - 2\sigma(t, T_p - \tau; j,k)]/\sigma(t, T_p; j,k), \tag{37}
$$

where the argument notation j and k has been added to denote the polarization components.

Section 5 provides sample calculations of time/speckle-spectrum signatures [Equation (27)], time-resolved cross-section distributions [Equation (35)], structure functions [Equation (36)] and normalized structure functions [Equation (37)] for various cone incident angles and target roughnesses.

5. COMPUTED RESULTS

The expressions outlined in Section 4.3 were computer coded to obtain numerical results for the signatures and structure functions, discussed in Sections 4.1 and 4.2, for a conical target. A cone with a 10° half angle was assumed, and a normalized base radius of unity was used in accord with the normalization (scaling) procedure discussed in Reference 12. All calculations assumed incident and scattered polarization vectors that were normal to the plane of incidence to the cone axis (i.e., HH). Four laser incident angles with respect to the cone axis (θ = 0°, 45°, 60°, 89°) and two roughness conditions were examined. A nominal surface-roughness condition corresponding to phenolic carbon scattering at 10.6 μm was employed which was determined from a ROSSCO[13] analysis of actual laser scattering data.[14] The derived ROSSCO parameters are

Normal Phenolic Carbon

$k\sigma = 0.529$, $k\ell = 2.72$, $s = 0.246$, $m = 4.0$, $n = 1.49$, $\alpha = 6.47 \times 10^{-3}$.

A smoother phenolic carbon material was examined with the following ROSSCO parameters:

Smooth Phenolic Carbon

$k\sigma = 0.529$, $k\ell = 5.0$, $s = 0.1$, $m = 4.0$, $n = 1.49$, $\alpha = 6.47 \times 10^{-3}$.

A pulse width, T_p, of 0.33 (in units of the normalized radius, x) was assumed, and normalized time intervals beginning at zero at the nearest range of the conical target were used. Computed results are presented and discussed in the following subsections.

5.1 Time/Speckle-Spectrum Signatures

Computed, ideal (i.e., noise-free) time/speckle-spectrum signatures are illustrated three-dimensionally in Figures 5, 6, 7, and 8 for the 0°, 45°, 60°, and 89° incident angles, respectively. Only positive values of x are depicted because the calculated signature is symmetric (i.e., the values of $d\sigma/dx$ for negative x values are mirror images of the values for positive x). The spectral width illustrated in Figure 5 for the 0° incident angle is somewhat fictitious because a normalization constant of zero (sin θ) multiplies the x axis. Nevertheless, a signature similar to the computed one is expected for nearby incident angles.

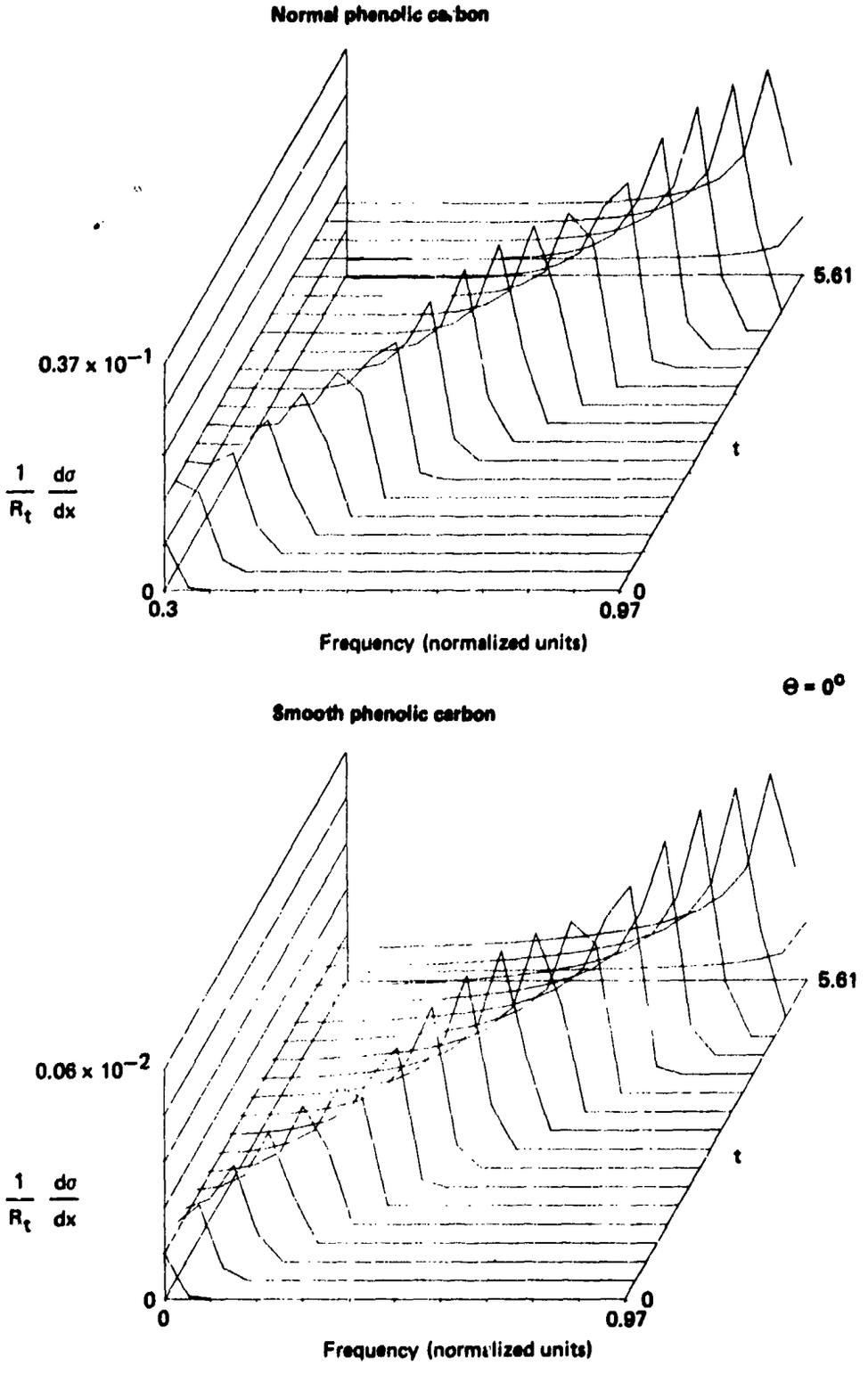

Figure 5 Time/speckle-spectrum signature for phenolic carbon cone (Θ = 0°)

GP77-0007-17

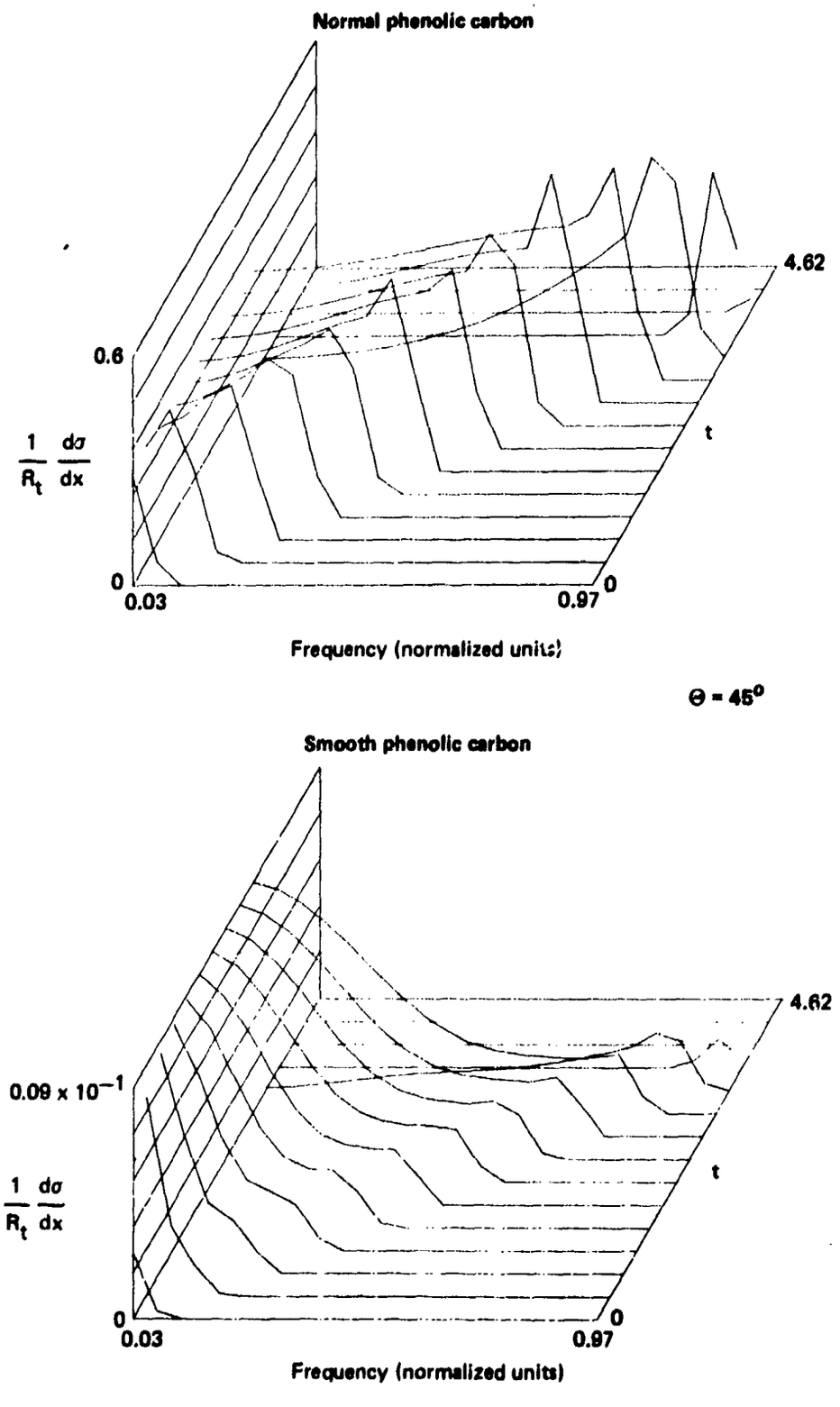

Figure 6 Time/speckle-spectrum signature for phenolic carbon cone ($\Theta = 45^o$)

GP77-0007-16

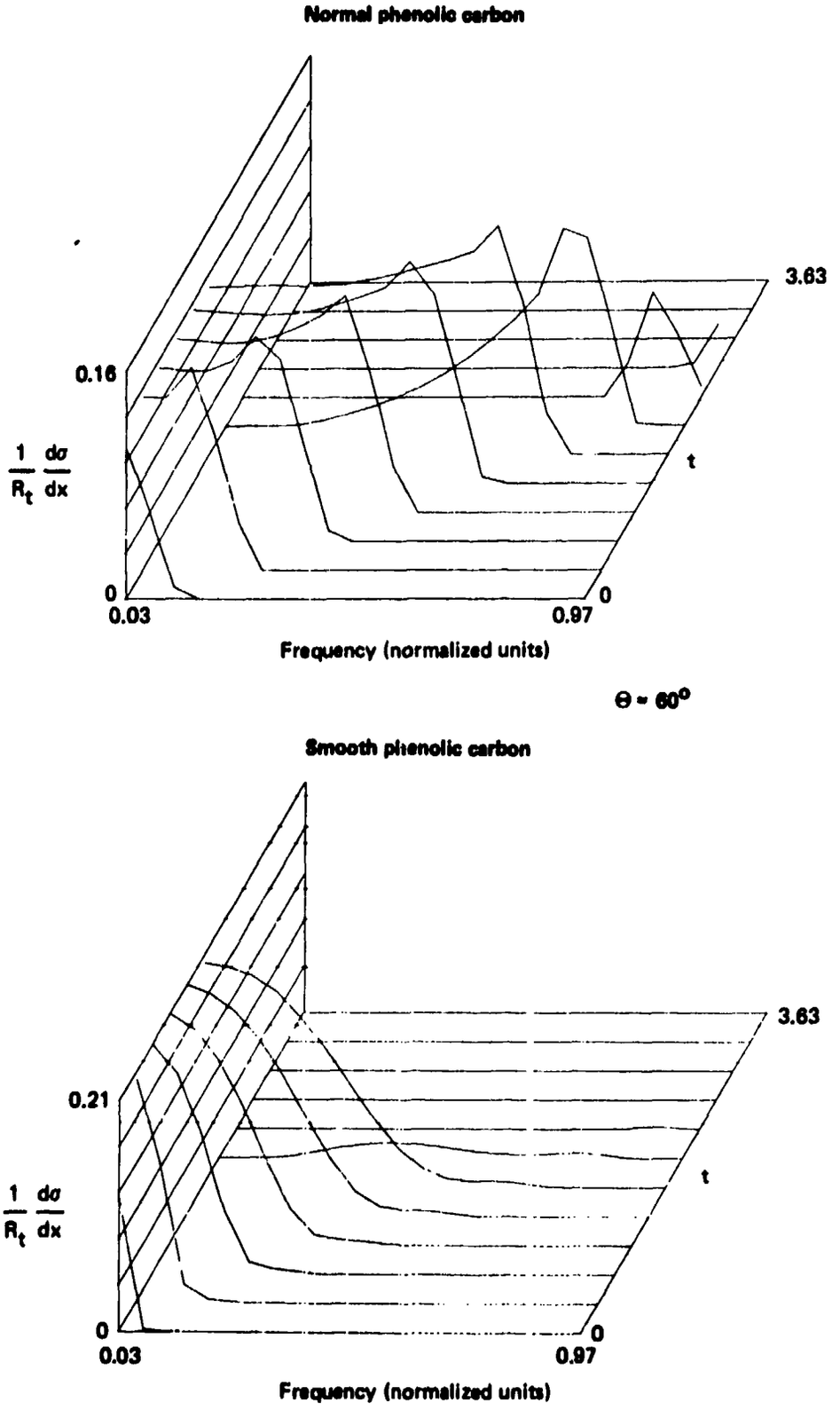

Figure 7 Time/speckle-spectrum signature for phenolic carbon cone (Θ = 60°)

GP77-0027-16

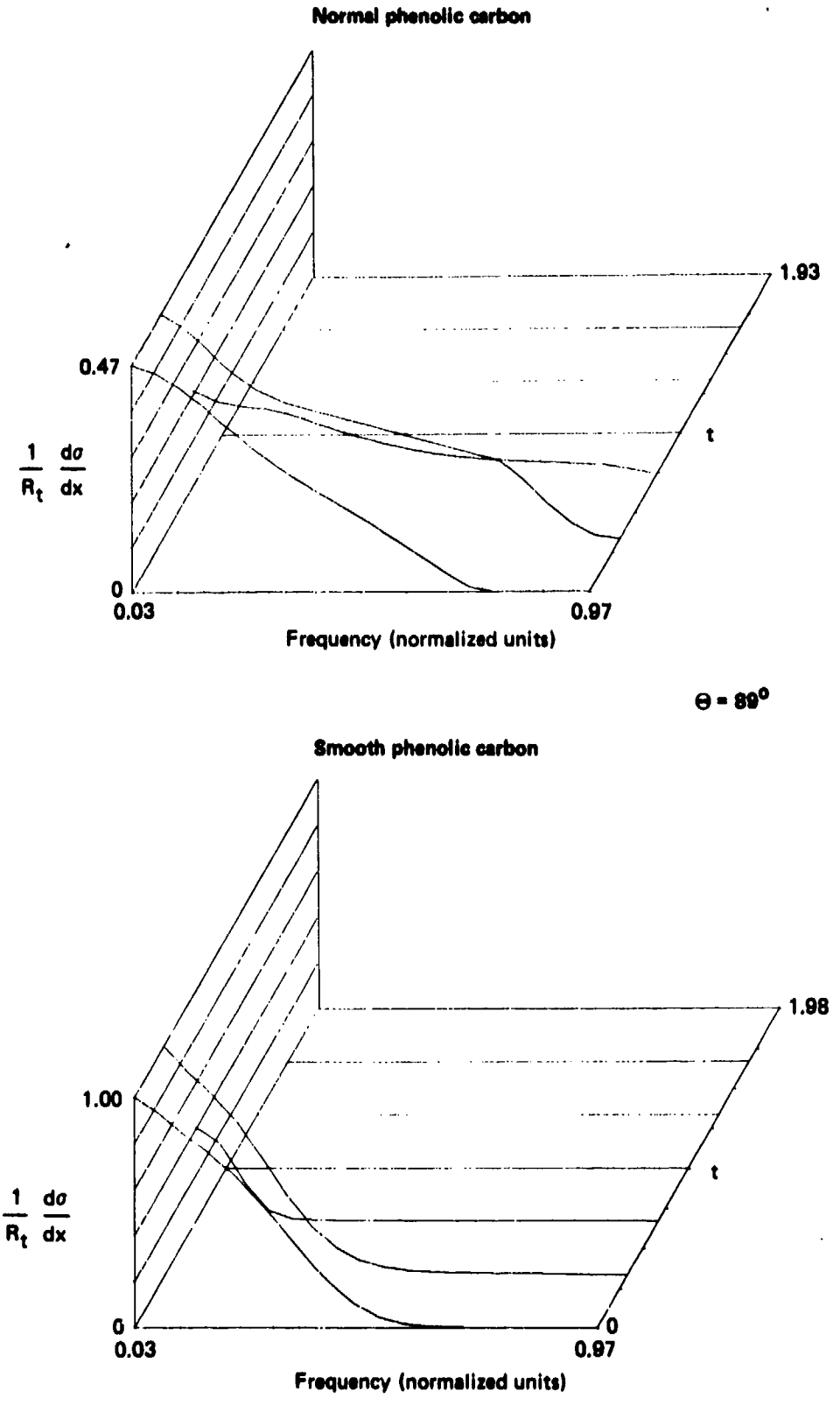

Figure 8 Time/speckle-spectrum signature for phenolic carbon cone (Θ = 89°)

GP77-0697-16

Two general observations concerning the calculated signatures can be made. First, it is noteworthy that for incident angles near nose-on ($\Theta = 0°$), the increased scattering area from the edge of the cone enhances the edge definition. This effect persists to an incident angle of 60° for carbon phenolic of normal roughness. Secondly, the effects of surface roughness (other than affecting the cross-section magnitude) become more pronounced for larger angles of incidence with respect to the cone axis. The aforementioned edge enhancement (resulting from the increased scattering area) is effectively eliminated by the smoother phenolic carbon for an incident angle of 45°. The numerical results indicate that it is doubtful if the edge of the smooth target can be resolved for angles of incidence of 60° or greater.

5.2 Time-Resolved Cross Sections

Computations of the time-resolved cross section [Equation (35)] for the four incident angles of interest are illustrated in Figures 9 - 12 for a time resolution of $\Delta t = 0.05$ (normalized units). It is noteworthy that deviations from a ramp distribution are observed as the incident angle increases and that the surface roughness alters the shape of the distribution for the larger incident angles.

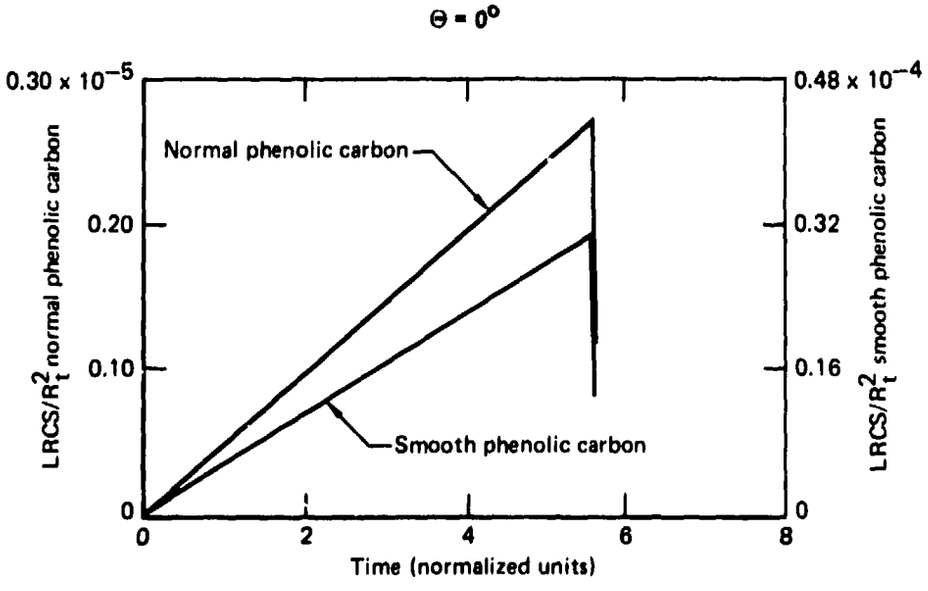

Figure 9 Time-resolved cross section for phenolic carbon cone ($\Theta = 0°$)

GP77-0007-7

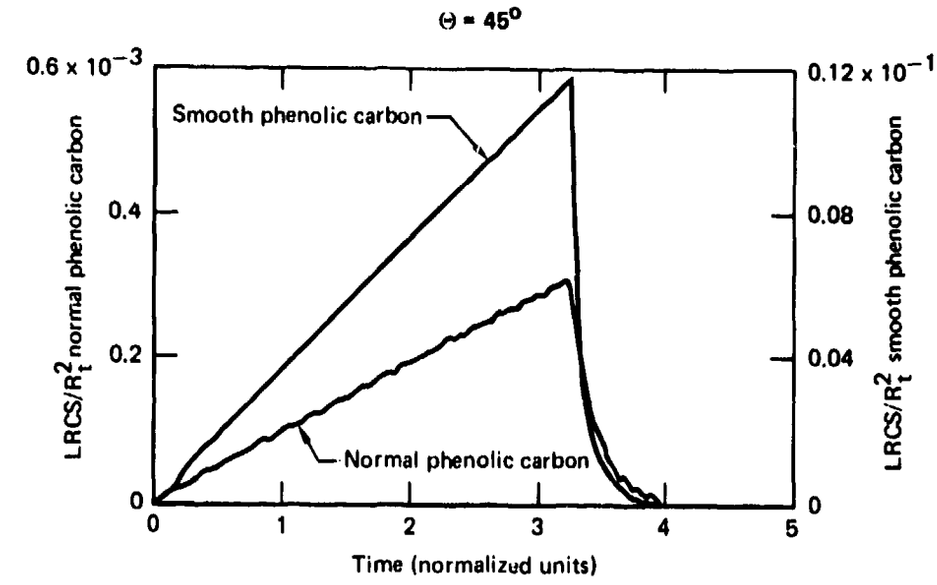

Figure 10 Time-resolved cross sections for phenolic carbon cone (Θ= 45°)

GP77-0997-9

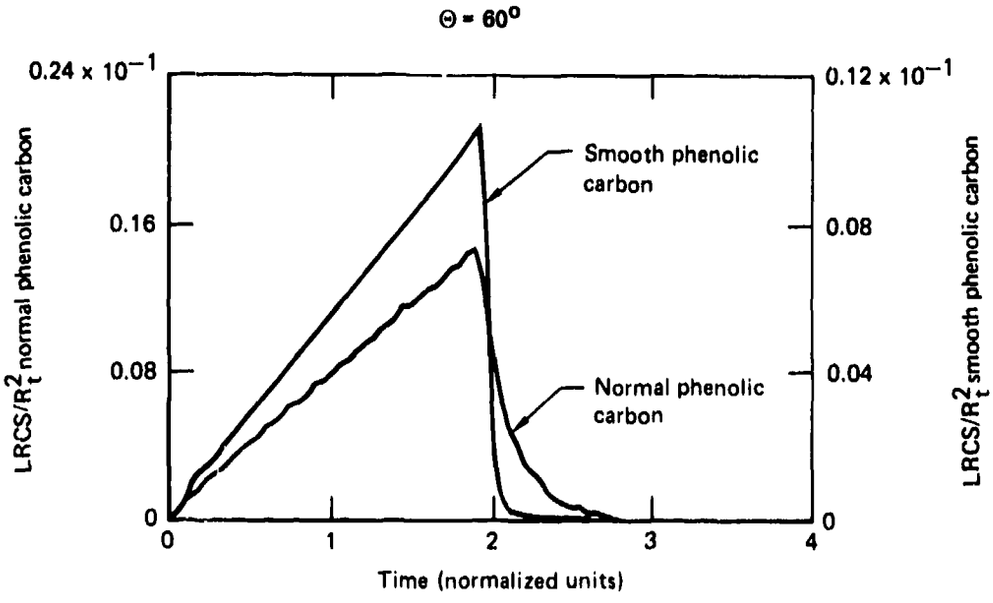

Figure 11 Time-resolved cross section for phenolic carbon cone (Θ = 60°)

GP77-0997-10

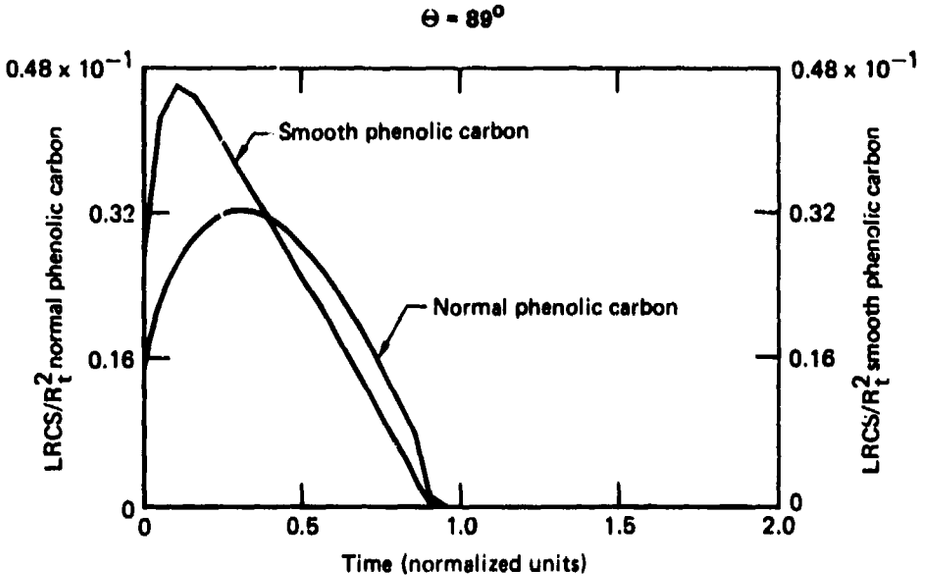

Figure 12 Time-resolved cross section for phenolic carbon cone (Θ = 89°)

GP77-0007-8

5.3 Cone Structure Functions

Calculated cone-structure functions [Equation (34) in units of LRCS/R_t^2 and τ/T_p] are illustrated in Figures 13 - 16 for the four incident angles of interest and various normalized times. Although the incident angle, time, and roughness condition alter the magnitude of the structure function at the time delay $\tau/T_p = 1$, the functional form of the structure function for values of $\tau/T_p < 1.0$ is unaltered by these factors even though the time-resolved LRCS is changed significantly (see Section 5.2). Clearly, a linear functional form approximates the structure function for values of $\tau/T < 1.0$ for all of the parameters investigated. Therefore, according to Equations (10) - (12) the power spectrum of fluctuations is of the form

$$H_{W_e}H(\omega) = \left[K \frac{\sin(\omega T_p/2)}{(\omega T_p/2)}\right]^2 . \qquad (38)$$

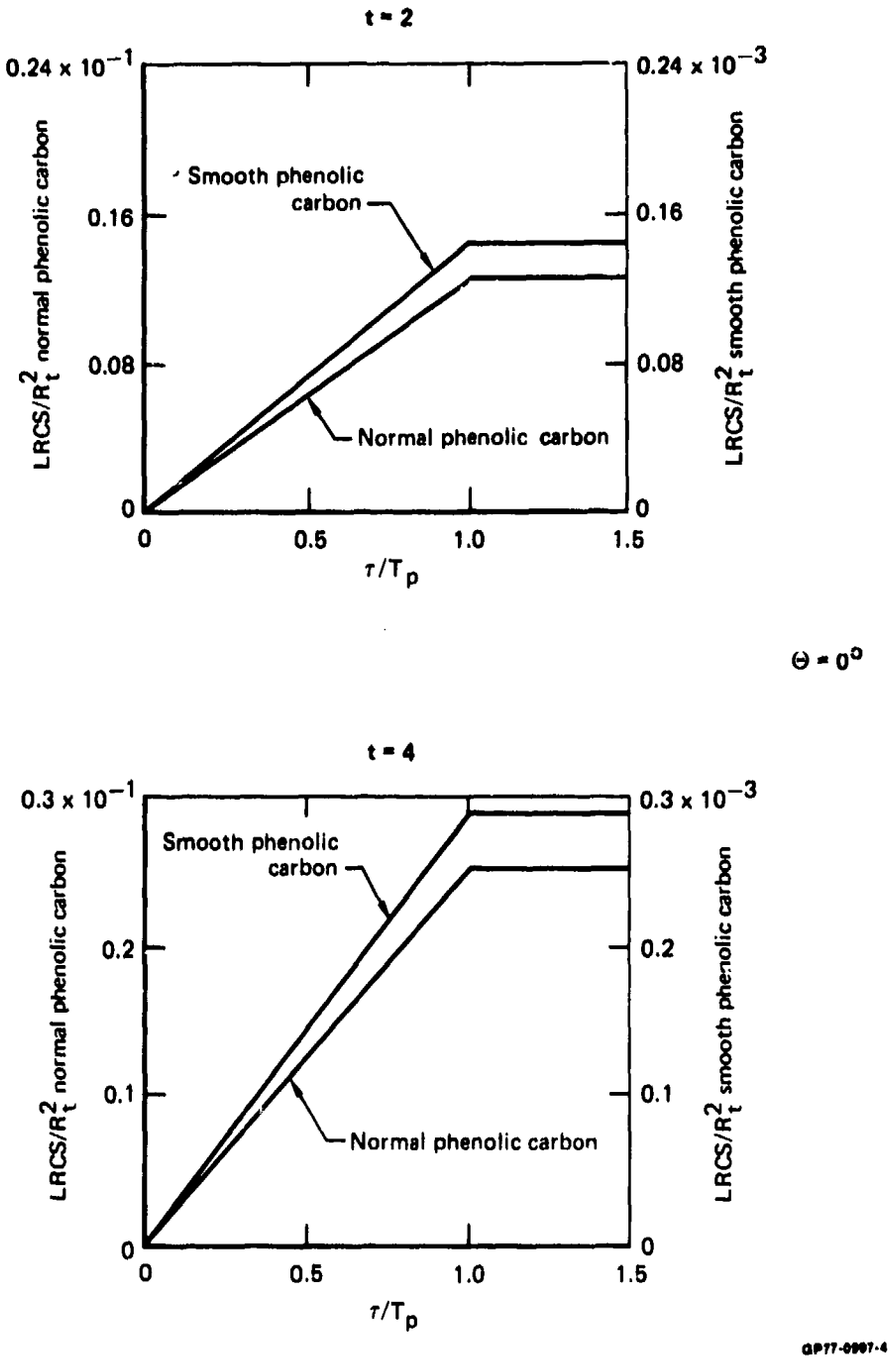

Figure 13 Pulse structure functions for phenolic carbon cone ($\Theta = 0^{o}$)

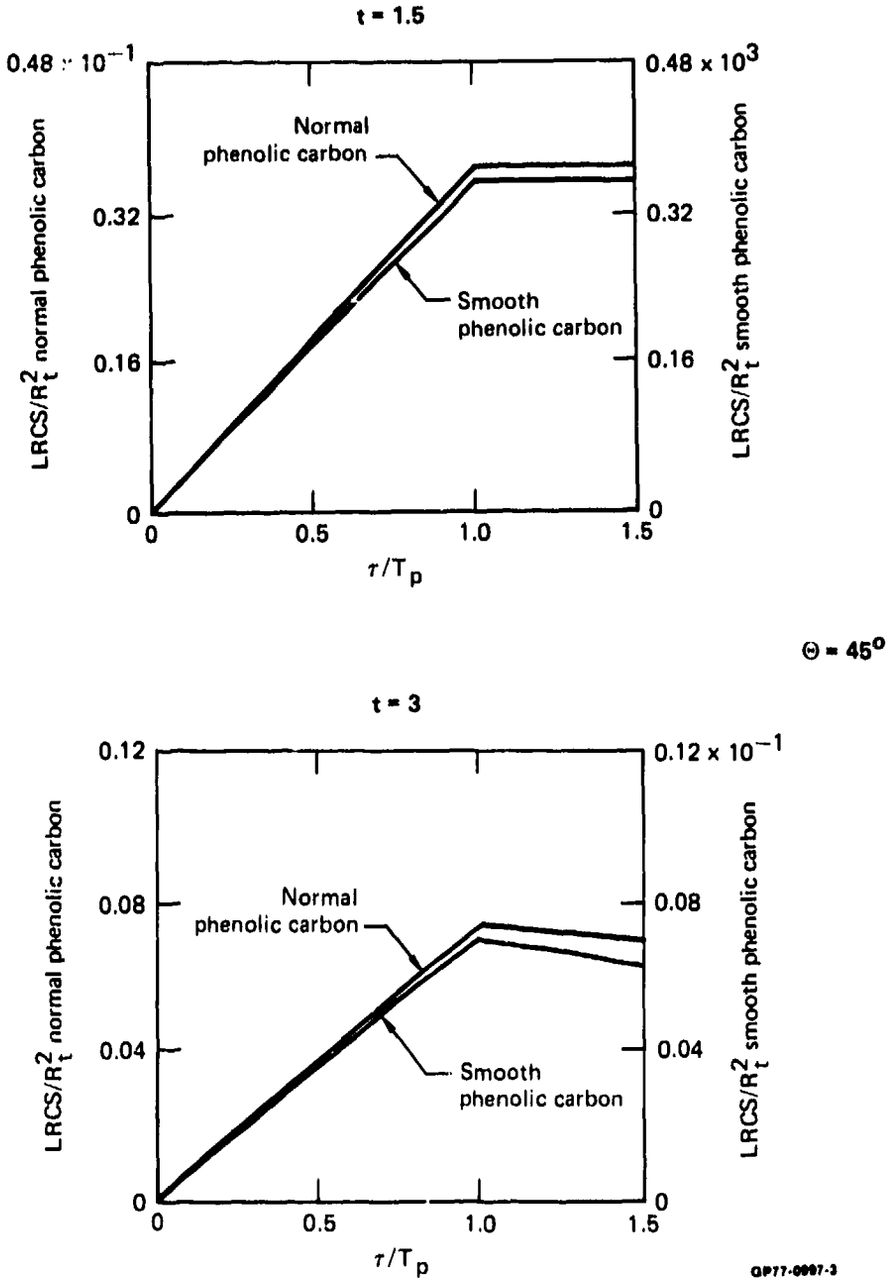

Figure 14 Pulse structure functions for phenolic carbon cone ($\Theta = 45^{o}$)

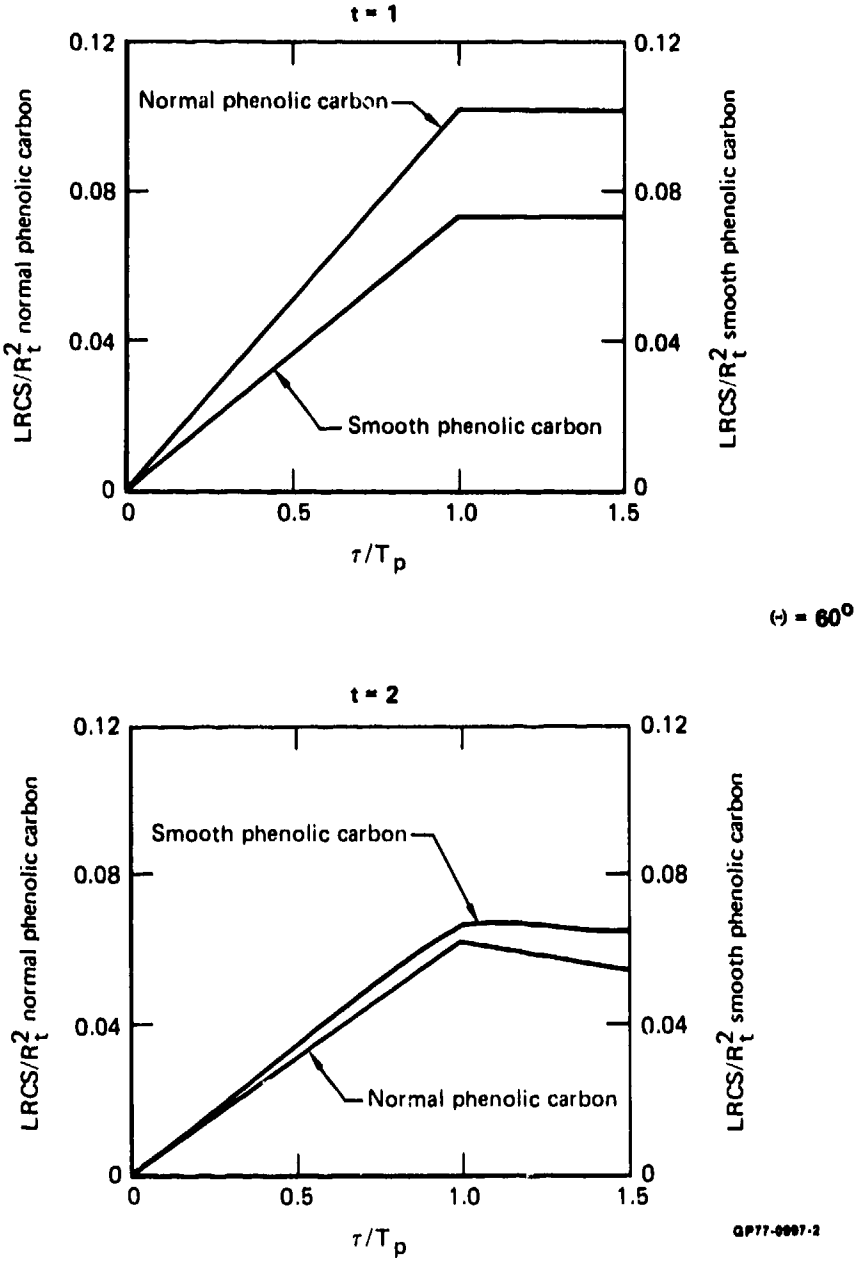

Figure 15 Pulse structure functions for phenolic carbon cone ($\Theta = 60^{o}$)

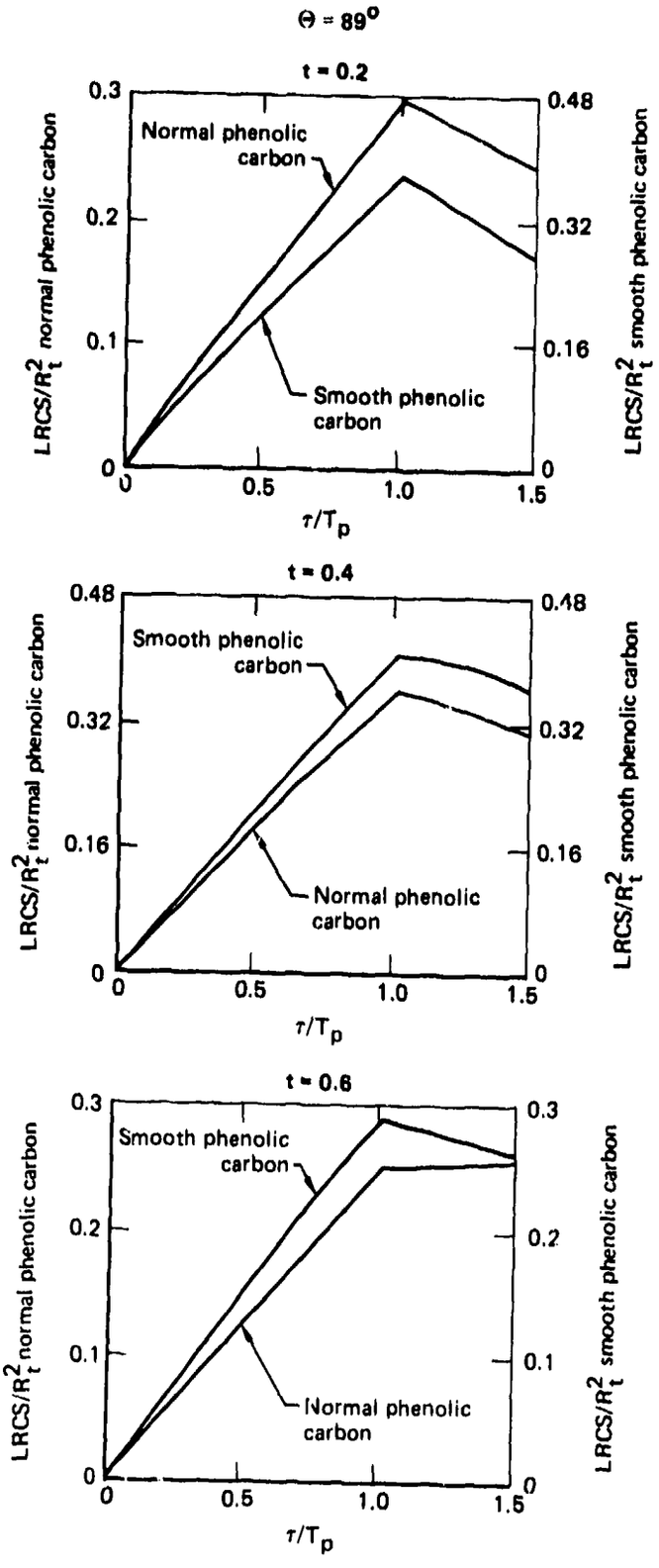

Figure 16 Pulse structure functions for phenolic carbon cone (Θ = 89°)

5.4 Normalized Cone-Structure Functions

Normalized cone-structure functions were calculated using the Equation (37) definition for various incident angles and roughness conditions. Representative results for the more interesting cases (i.e., large incident angles) are shown in Figures 18 and 19 to illustrate the effectiveness of the normalization adopted in the definition of the normalized structure function. Although the approximate linear functional form (for $\tau/T_p < 1$) noted in the previous section is unaltered by the normalization, the slopes of the structure functions in general have been approximately equated by the normalization procedure. Thus, it may reasonably be concluded that homogeneous conical targets possess normalized statistical local homogeneity (as defined in Section 4.2). Subsequent calculations of intra-pulse speckle effects on the time/speckle-spectrum signatures of cones are considerably simplified by this fact.

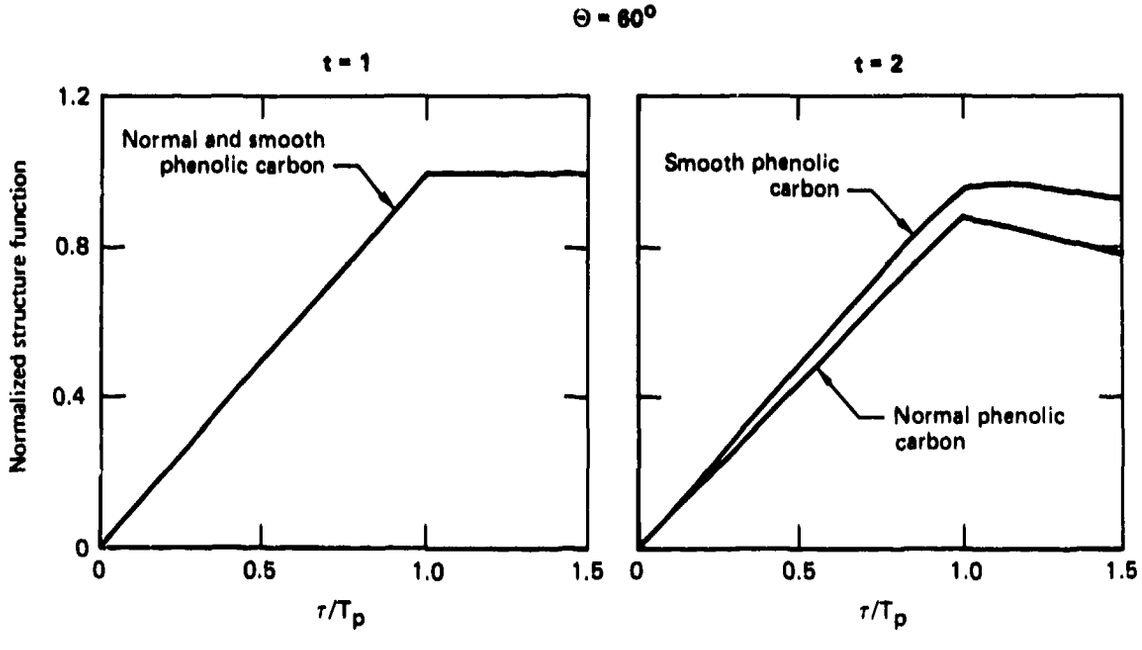

Figure 17 Normalized pulse structure functions for phenolic carbon cone (Θ = 60°)

GP77-0007-6

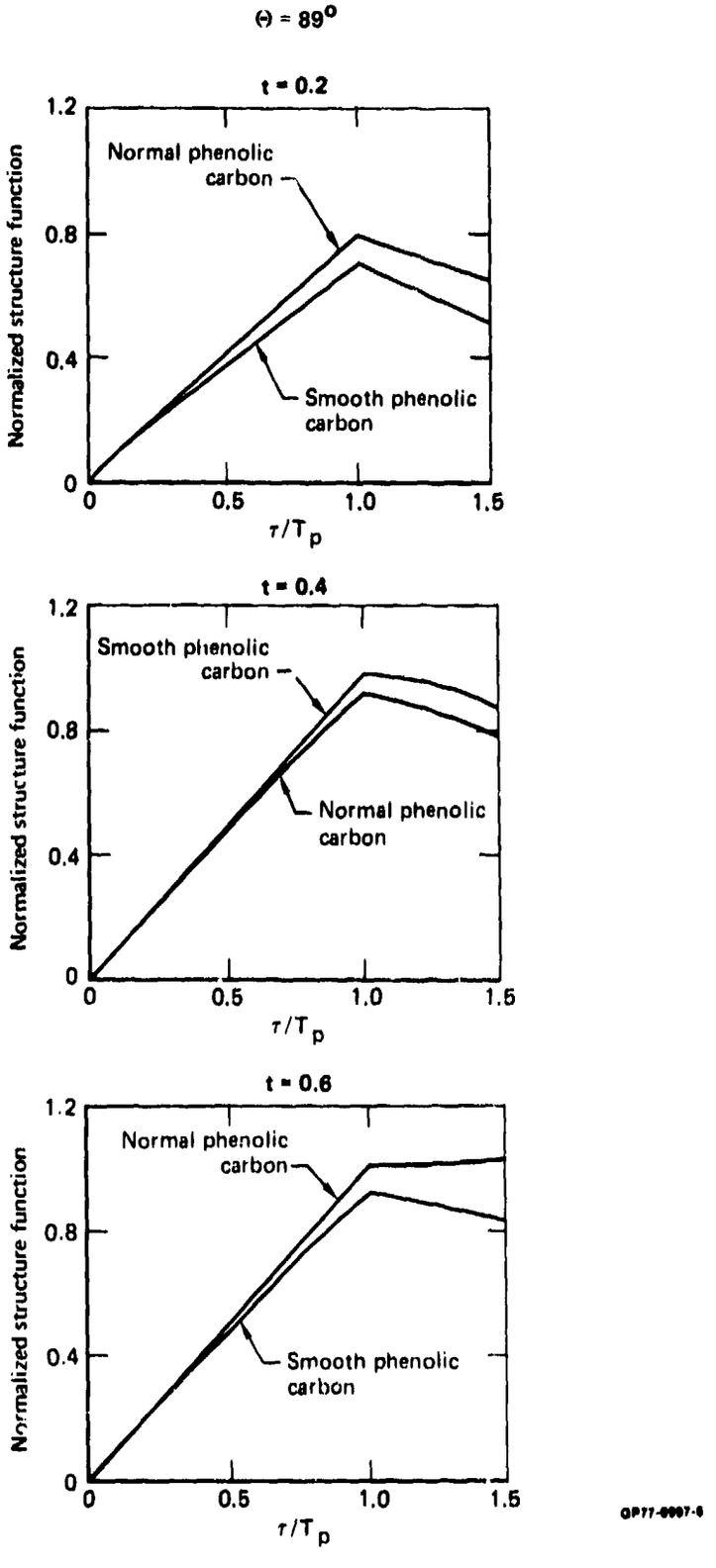

Figure 18 Normalized pulse structure functions for phenolic carbon cone (Θ = 89°)

REFERENCES

1. L. R. Tomasetta, G. M. Carter, and M. S. Edelstein, Wideland 10.6 μm Backscatter Range, Lincoln Laboratory Interim Project Report, Report #ESD-TR-76-321, Electronic Systems Division Contract F19628-76-C-0002, 2 November 1976.
2. J. C. Leader, An Analysis of the Spatial Coherence of Laser Light Scattered from a Surface with Two Scales of Roughness, J. Opt. Soc. Am. 66, 536 (1976).
3. J. C. Leader, Spatial Coherence Measurements of Rayleigh-Scattered Light, J. Opt. Soc. Am. 65, 740 (1975).
4. J. C. Leader, An Analysis of the Frequency Spectrum of Laser Light Scattered from Moving Rough Objects, J. Opt. Soc. Am. 67, 1091 (1977).
5. A. M. Yaglom, Stationary Random Functions (Prentice-Hall, Inc., Englewood Cliffs, NJ, 1962).
6. J. C. Leader, Laser Signature Analyses, McDonnell Douglas Report MDC Q0611, Interim Report, BMDATC Contract No. DASG60-76-C-0041, 22 October 1976.
7. P. Beckmann and A. Spizzichino, The Scattering of Electromagnetic Waves from Rough Surfaces (Pergamon Press, Oxford, 1963).
8. J. Ohtsubo and T. Asakura, Statistical Properties of Laser Speckle Produced in the Diffraction Field, Appl. Opt. 16, 1742 (1977).
9. W. B. Davenport and W. L. Root, Random Signals and Noise (McGraw Hill, New York, 1958).
10. op. cit., Reference 5., p 87
11. V. I. Tatarski, Wave Propagation in a Turbulent Medium, (Dover, New York, 1961).
12. J. C. Leader, Laser Radar Cross Section Analyses, McDonnell Douglas Report MDC Q0585, Final Report, BMDATC Contract No. DASG60-75-C-0051, 24 January 1976.
13. J. C. Leader and J. M. Putnam, Rough Surface Scattering Code (ROSSCO) User's Manual, McDonnell Douglas Report MDC Q0619, Vol. I, Program Description, BMDATC Contract No. DASG60-76-C-0041, 22 May 1977.
14. J. P. Theriault and W. S. Otaguro, Monostatic BDR Measurements of BMD Materials, McDonnell Douglas Report MDC G6128, September 1976.

DISTRIBUTION LIST

Addressees	Cys
Director Ballistic Missile Defense Advanced Technology Center ATTN: ATC-O/E. Sanmann, L. Hayes, M. Lavin, J. Hagelstration; ATC-D, ATC-R, ATC-P P.O. Box 1500 Huntsville, AL 35807	1EA
Ballistic Missile Defense Program Office ATTN: DASC-BMT, C. McLain 1300 Wilson Boulevard Arlington, VA 22209	1
Director Defense Advanced Research Projects Agency Strategic Technology Office ATTN: A. Pike 1400 Wilson Boulevard Arlington, VA 22209	1
Defense Documentation Center Cameron Station Alexandria, VA 22314	2
Commander Air Force Avionics Laboratory ATTN: AFAL/WRP; AFAL/LPJ Wright Patterson AFB, OH 45433	1EA
Director Defense Research & Engineering Department of Defense The Pentagon ATTN: R. Yost Washington, DC 20301	1
Commander Air Force Geophysical Labs L. G. Hanscom Field ATTN: John S. Garing Redford, MA 01730	1

Addressees	Cys
Director Naval Research Laboratory (EOTP) ATTN: G. L. Harvey 4855 Overlook Drive Washington, DC 20301	1
Director Naval Surface Weapons Center ATTN: C. Infisino, Code WD-21 White Oak, MD 20910	1
Commander Rome Air Development Center ATTN: F. J. Demma Griffiss AFB, NY 13441	1
U.S. Department of Commerce National Bureau of Standards ATTN: R. L. Smith Electromagnetic Div. Boulder, CO 80302	1
Commander Space & Missile Systems Organization ATTN: MAJ S. Bevens P. O. Box 92960 Worldway Postal Center Los Angeles, CA 90009	1
Commander U.S. Army Missile R & D Command ATTN: DRDMI-HRQ/J. Stettler, W. Gamble; DRDMI-H/ R. Conrad Redstone Arsenal, AL 35809	1EA
Aeronutronic-Ford Corporation Ford Road ATTN: R. D. Reid New Port Beach, CA 92663	1
Aerospace Corporation ATTN: R. Strickler P. O. Box 95085 Los Angeles, CA 90045	1

Addressees	Cys
Calspan Corporation ATTN: R. E. Kell, J. Grace P. O. Box 235 Buffalo, NY 14221	1EA
CINDAS Purdue Industrial Research Park ATTN: Y. S. Touloukian 2595 Yeager Road West Lafayette, IN 47906	1
Environmental Research Institute of Michigan (ERIM) ATTN: G. Zissis P. O. Box 618 Ann Arbor, MI 48107	1
General Electric Company TEMPO Division ATTN: M. Stanton; T. Stevens 816 State Street Santa Barbara, CA 92101	1EA
General Electric Company Valley Forge Space Center ATTN: J. Burns P. O. Box 8555 Philadelphia, PA 19101	1
General Research Corporation Washington Operations ATTN: G. F. Gurski 7655 Old Springhouse Road McLean, VA 22101	1
Honeywell, Incorporated Systems Research Center ATTN: R. Heinisch, M.S. R2340 2600 Ridgway Parkway Minneapolis, MN 55413	1
Hughes Aircraft Company ATTN: Sam Vodopia Bldg. 61C129 Culver City, CA 90230	2
Hughes Aircraft Company ATTN: R. Kafka Bldg. 606/K235 P. O. Box 3310 Fullerton, CA 92634	1
Intelcom Rad Tech ATTN: T. Neu P. O. Box 80817 San Diego, CA 92138	1
McDonnell Douglas Corporation Holiday Office Center ATTN: H. L. Herdman 3322 Memorial Parkway Huntsville, AL 35804	1
McDonnell Douglas Corporation ATTN: L. E. Gernert H. Rose, A3-362 MS 13-2 S. Spirak J. Grossman 5301 Bolsa Avenue Huntington Beach, CA 92647	1EA
MIT Lincoln Laboratory ATTN: R. Kingston, S. Edelburg, P. Longaker, L. R. Tomasetta, G. M. Carter M. S. Edelstein P. O. Box 73 Lexington, MA 02173	1EA
Riverside Research Institute ATTN: M. King 80 West End Avenue New York, NY 10023	1
Taylor-Jamron Services ATTN: R. Jamron 1741 Weldon Boulevard Ann Arbor, MI 48103	1

Addressees	Cys
Teledyne Brown Engineering ATTN: N. Passino 300 Sparkman Drive Huntsville, AL 35807	1
TRW Systems, RI-1038 ATTN: J. Fox One Space Park Redondo Beach, CA 90278	1
L'Carde, Inc. ATTN: M. Thomas 1555 Palentia Avenue Newport Beach, CA 92660	1
Spartan Research Associates ATTN: J. J. Geanakos P. O. Box 6346 Orange, CA 92667	1
Boeing Aerospace Company ATTN: George Thacker M.S. 87-43 P. O. Box 3999 Seattle, WA 98124	1
Rockwell International Missile Systems Division ATTN: T. W. Donaven D/646, DC 22 P. O. Box 4182 3370 Miraloma Avenue Anaheim, CA 92803	1
R&D Associates Suite 1100 ATTN: Frank Sevcik 1815 North Fort Myer Drive Arlington, VA 22209	1

Addressees	Cys
Institute for Defense Analyses ATTN: Documents Acquisitions 400 Army Navy Drive Arlington, VA 22202	1
Optical Science Co. ATTN: D. Fried P. O. Box 388 Yorba Linda, CA 92686	1
United Technologies Research Center ATTN: A. Vuylsteke 400 Main Street East Hartford, CT 06108	1
Commander Rome Air Development Center ATTN: R. Ogrodnik J. Michaels Griffiss AFB, NY 13441	1EA
California Institute of Technology ATTN: Nicholas George Pasadena, CA 91125	1
Air Force Weapons Laboratory ATTN: B. Hogge AFWL-ALO Kirtland AFB, NM 87117	1
Optical Sciences Center University of Arizona ATTN: W. Wolfe Tucson, Arizona 85721	1